Amorphous MoS_3 as the sulfur-equivalent cathode material for room-temperature Li–S and Na–S batteries

Hualin Ye[a,1], Lu Ma[b,1], Yu Zhou[a], Lu Wang[a], Na Han[a], Feipeng Zhao[a], Jun Deng[a], Tianpin Wu[b], Yanguang Li[a,2], and Jun Lu[b,2]

[a]Institute of Functional Nano and Soft Materials, Jiangsu Key Laboratory for Carbon-Based Functional Materials and Devices, Soochow University, Suzhou 215123, China; and [b]Chemical Sciences and Engineering Division, Argonne National Laboratory, Lemont, IL 60439

Edited by Richard Eisenberg, University of Rochester, Rochester, New York, and approved October 31, 2017 (received for review July 3, 2017)

Many problems associated with Li–S and Na–S batteries essentially root in the generation of their soluble polysulfide intermediates. While conventional wisdom mainly focuses on trapping polysulfides at the cathode using various functional materials, few strategies are available at present to fully resolve or circumvent this long-standing issue. In this study, we propose the concept of sulfur-equivalent cathode materials, and demonstrate the great potential of amorphous MoS_3 as such a material for room-temperature Li–S and Na–S batteries. In Li–S batteries, MoS_3 exhibits sulfur-like behavior with large reversible specific capacity, excellent cycle life, and the possibility to achieve high areal capacity. Most remarkably, it is also fully cyclable in the carbonate electrolyte under a relatively high temperature of 55 °C. MoS_3 can also be used as the cathode material of even more challenging Na–S batteries to enable decent capacity and good cycle life. *Operando* X-ray absorption spectroscopy (XAS) experiments are carried out to track the structural evolution of MoS_3. It largely preserves its chain-like structure during repetitive battery cycling without generating any free polysulfide intermediates.

Li–S battery | Na–S battery | amorphous MoS_3 | carbonate

There has been an increasing demand for the development of advanced battery technologies with high energy/power density, long cycle life, and low cost (1, 2). Among all promising solutions, lithium–sulfur (Li–S) batteries have attracted particular attention by virtue of the large theoretical capacity (1,675 mAh/g) of sulfur, its low cost (<$150/ton), and earth abundance (3–8). However, Li–S batteries have not reached their expected potential. Firstly, sulfur cathodes are not compatible with carbonate-based electrolytes commonly used in lithium-ion batteries. Their polysulfide intermediates readily react with carbonates via a nucleophilic addition or substitution reaction, leading to a sudden capacity fading (7–10). While ether-based electrolytes, such as the combination of 1,3-dioxolane/1,2-dimethoxyethane, DOL/DME) have no such problem, they are more volatile and restrict the actual working temperature of batteries below 50 °C (9, 11). Secondly, polysulfides have considerable solubility in ether-based electrolytes and are prone to escape from the cathode during discharge. These species not only markedly reduce the active material utilization and the Coulombic efficiency, but also corrode the lithium metal when diffusing to the anode (6–8). Having analogous electrochemistry to Li–S batteries, room-temperature sodium–sulfur (Na–S) batteries have also been proposed but are even more problematic (12–15). They suffer from a serious cycling problem. At present, there are very few reports about cyclable Na–S batteries (12).

To tackle these issues, different strategies have been developed under one similar guiding principle: to keep polysulfides at the cathode and to diminish their dissolution in the electrolyte (6–8). Most recent studies use various functional electrode components to trap polysulfides, including but not limited to carbonaceous materials (porous carbon, graphene oxide, carbon nanotube, etc.) (16–19), metal oxides (TiO_2, Al_2O_3, V_2O_5, MoO_3, MnO_2, etc.) (20–24), disulfides (TiS_2, ZrS_2, VS_2, etc.) (23, 25, 26), hydroxides [$Ni(OH)_2$, etc.] (27, 28), and polymers (polyaniline, polypyrrole, polyacrylonitrile, and so on) (29, 30). Considerable research efforts have also been invested in the proper design and functionalization of battery separators to suppress the shuttling of polysulfides between the cathode and anode (31–33). Nevertheless, few of these practices are proven fully effective. The auxiliary blocking materials introduced are usually electrochemically inert. They not only dilute the content of electrochemically active sulfur in the working cathode (sometimes <40 wt %), but often create extensive voids that seriously limit battery areal and volumetric capacities below practical values (5, 34). To make it even worse are the complexity and fabrication cost added by these practices, which essentially go against the original motivation for using sulfur cathodes.

Alternatively, the possibility of using organic sulfides (such as tetramethylthiuram disulfide and 2,5-dimercapto-1,3,4-thiadiazole) has also been pursued for decades (35–38). In these compounds, sulfur is covalently bonded to the carbon chain, and does not detach from the electrode material even at full discharge (35, 36). Nevertheless, they are generally not considered for practical applications due to their high solubility in organic electrolytes, inferior electronic conductivity, and low sulfur content (5, 7, 9, 34).

Here, we reason that analogous to organic sulfides, sulfur-containing inorganic compounds (such as transition metal sulfides and polysulfides) may hold unexpected promise as the "sulfur-equivalent" cathode materials. By sulfur-equivalent we expect that these materials do not contain elemental sulfur but exhibit sulfur-like electrochemical behaviors. Our interest in them lies in the possibility that their reaction pathways may not involve the formation of soluble polysulfide intermediates. This may circumvent all

Significance

We propose a concept of "sulfur-equivalent cathode materials," and reason that instead of using problematic elemental sulfur, one can use sulfur-containing compounds as the alternatives with a comparable electrochemical property but free of any polysulfide generation. We demonstrate here the great potential of amorphous MoS_3 as such a sulfur-equivalent cathode material for room-temperature Li–S and Na–S batteries. More remarkably, we find that MoS_3 is fully cyclable in the carbonate electrolyte (which is known to kill conventional sulfur cathodes) under a relatively high temperature of 55 °C. MoS_3 can also be used as the cathode material of even more challenging Na–S batteries to enable an impressive performance.

Author contributions: Y.L. and J.L. designed research; H.Y., L.M., Y.Z., L.W., and N.H. performed research; F.Z., J.D., and T.W. contributed new reagents/analytic tools; and H.Y., Y.L., and J.L. wrote the paper.

The authors declare no conflict of interest.

This article is a PNAS Direct Submission.

[1]H.Y. and L.M. contributed equally to this work.

[2]To whom correspondence may be addressed. Email: yanguang@suda.edu.cn or junlu@anl.gov.

This article contains supporting information online at www.pnas.org/lookup/suppl/doi:10.1073/pnas.1711917114/-/DCSupplemental.

of the long-standing issues of conventional Li–S and Na–S batteries, and ultimately lead to excellent battery cycle life necessary for the commercialization of sulfur batteries. However, not all sulfur-containing inorganic compounds can be considered as sulfur-equivalent. There are two important criteria as outlined below. They should have a high working voltage akin to sulfur (~2 V for Li–S). They should also contain a high sulfur content (>40 wt %) to rival conventional sulfur cathodes.

Results and Discussion

MoS_2 was taken as the starting point to test our proposal because it is one of the most popular transition-metal sulfides for energy conversion and storage (39, 40). MoS_2 consists of covalently bonded monolayers brought together by weak van der Waals interactions—a structure analogous to graphite (Fig. 1*A*, *Inset*). It has been traditionally considered as the anode material of lithium-ion or sodium-ion batteries (39, 41, 42). Here, we assessed its performance as the sulfur-equivalent cathode material for Li–S batteries, and applied a lower cutoff voltage of 1.2 V versus Li^+/Li. No appreciable capacity was measured when MoS_2 was directly cycled between 1.2 and 3.0 V versus Li^+/Li (Fig. 1*A*). This was not surprising since the intercalation of Li^+ ions into MoS_2 interlayers was known to take place at ~1.1 V (42, 43). Interestingly, we found that if MoS_2 was initially discharged down to 0.01 V (a process defined as "activation"), it then featured a discharge plateau around 1.9 V at all subsequent cycles (Fig. 1*B*). Such an observation was consistent with previous results and indicative of a permanent structure change during the first discharge even though its exact cause remained a topic of constant debate (40, 43–46). The specific capacity between 1.2 and 3.0 V at the second cycle reached 277 mAh/g when normalized to the total mass of MoS_2. Even though its discharge voltage was close to that of elemental sulfur, we believed that the specific capacity measured here was insufficient to render MoS_2 appealing as the sulfur-equivalent cathode material for Li–S batteries.

We next explored the potential of the cousin material of MoS_2—amorphous MoS_3. MoS_3 was proposed to have a chain-like structure consisting of Mo ions bridged by sulfide and disulfide ligands as schematically illustrated by the Fig. 2*A*, *Inset* (47, 48). Its electrochemical lithiation and delithiation was first studied about four decades ago (49–51). Compared with crystalline layered MoS_2, amorphous chain-like MoS_3 has several structural advantages: it has higher sulfur content; its one-dimensional chain can facilitate the fast diffusion of Li^+ or Na^+ ions and has more open sites toward their active storage (52).

The preparation of MoS_3 followed the acid precipitation method using $(NH_4)_2MoS_4$ as the precursor in the presence of a small amount of multiwall carbon nanotubes (CNTs) as the conductive additive (see *Materials and Methods* for more details). We valued this synthetic method for its simplicity, reproducibility, and amenability to mass production. The X-ray diffraction (XRD) pattern of the final product was largely featureless except for a broad peak centered at ~14°, in good agreement with amorphous MoS_3 (53) (Fig. 2*A*). Its Raman spectrum had vibration bands of MoS_3 between 200 and 400 cm^{-1} as well as D and G bands from CNTs (54) (Fig. 2*B*). S 2p X-ray photoelectron spectroscopy (XPS) spectrum displayed a broad envelope of two doublets assignable to terminal or bridging (di)sulfide ligands—features characteristic of MoS_3 (55) (Fig. 2*C*). Moreover, the final product was examined under transmission electron microscopy (TEM). Fig. 2*D* is a representative low-magnification TEM image showing that the product had fiber-like morphology. It resulted from the deposition of MoS_3 on the CNT template. Close examination revealed that the MoS_3 coating was granular with an average size of ~20 nm. It had no obvious ordered lattice fringe, corroborating its amorphous nature (Fig. 2*E*). Brunauer–Emmett–Teller (BET) analysis suggested that MoS_3 had a low surface area (16.3 m^2/mg) and porosity (0.09 cm^3/g) (Fig. S1). From thermogravimetric analysis (TGA) in air, we concluded that the final product contained 11 wt % CNTs and ~45 wt % S (Fig. 2*F*). It was worth noting that the sulfur content measured here was no lower than many conventional sulfur composite materials containing 40 wt % S or even lower) that were designed to trap polysulfides (19, 56–60).

To evaluate the electrochemical performance of MoS_3 as the sulfur-equivalent cathode material for Li–S batteries, we paired it with a metallic Li foil in standard coin cells. The areal loading of MoS_3 was kept at ~2 mg/cm^2 unless otherwise noted. We first carried out battery measurements using the most popular ether electrolyte, i.e., 1 M lithium bis(trifluoromethanesulfonyl)imide (LiTFSI) in DOL/DME with the addition of 0.1 M $LiNO_3$. Fig. 3*A* illustrates the cyclic voltammetry (CV) curves of MoS_3 in the potential range of 1.2–3.0 V at 0.1 mV/s for the first three cycles. They featured two pairs of redox waves with the first cathodic wave centered at 1.84–1.87 V and the second cathodic wave centered at 1.31–1.36 V, suggesting a two-stage lithiation/delithiation process. Consistent results were also obtained from the galvanostatic charge/discharge experiments. The discharge curve of MoS_3 displayed a voltage plateau between 1.8 and 2.0 V, followed by a sloping tail down to the cutoff voltage of 1.2 V (Fig. 3*B*). The specific capacity delivered during the first cycle was 667 mAh/g when normalized to the total mass of MoS_3, and ~1,482 mAh/g when normalized to the sulfur weight. Most strikingly, amorphous MoS_3 exhibited an electrochemical behavior distinct from crystalline MoS_2 at the first cycle. It did not require an activation process to present the sulfur-like plateau around 1.9 V. In fact, the change in MoS_3 discharge curves before and after the first cycle was quite subtle (Fig. 3*B*). This comparison clearly underlined that the structural difference between two materials greatly impacted their initial lithiation pathway, and that amorphous MoS_3 likely preserved its chain-like structure during repeated cycling, which would be shown to be indeed so later by our *operando* synchrotron study.

The biggest challenge plaguing the development of Li–S batteries is their poor cycling stability due to the dissolution of polysulfide intermediates (8, 10). It was thereby one of the main pursuits in our study to evaluate the cycling stability of MoS_3. This sulfur-equivalent cathode material was galvanostatically charged and discharged at a specific current of 0.45 A/g. It exhibited a high initial specific capacity of 585 mAh/g, which gradually decreased over the first 200 cycles, then leveled off and stabilized (Fig. 3*C*). At the end of 1,000 cycles, it still retained a specific capacity of ~383 mAh/g. The Coulombic efficiency was in the range between 99.8~100.2% since the second cycles. Even though the reported specific capacity here appeared to be lower than most sulfur composites because it was normalized to the total mass of MoS_3, we argued that if the electrochemically inert components in the latter (for trapping polysulfides) was also counted (in fact they have to be counted), the practical specific

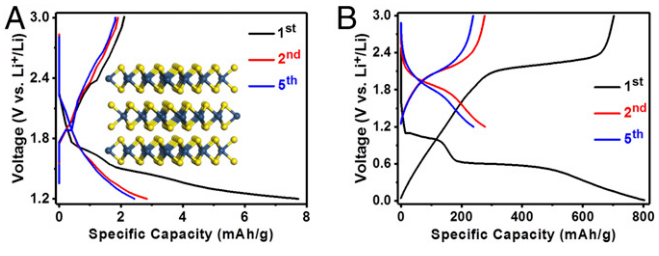

Fig. 1. Layered MoS_2 as the sulfur-equivalent cathode material for Li–S batteries. (*A*) Galvanostatic charge and discharge curves of MoS_2 between 1.2 and 3 V at 50 mA/g. (*Inset*) Schematic structure of 2D layered MoS_2, where the blue and yellow spheres represent Mo and S atoms, respectively. (*B*) Galvanostatic charge and discharge curves of MoS_2 with the initial cycle between 0.01 and 3 V (activation process), and subsequent cycles between 1.2 and 3 V at 50 mA/g. Under both testing conditions, MoS_2 exhibited small useful capacity.

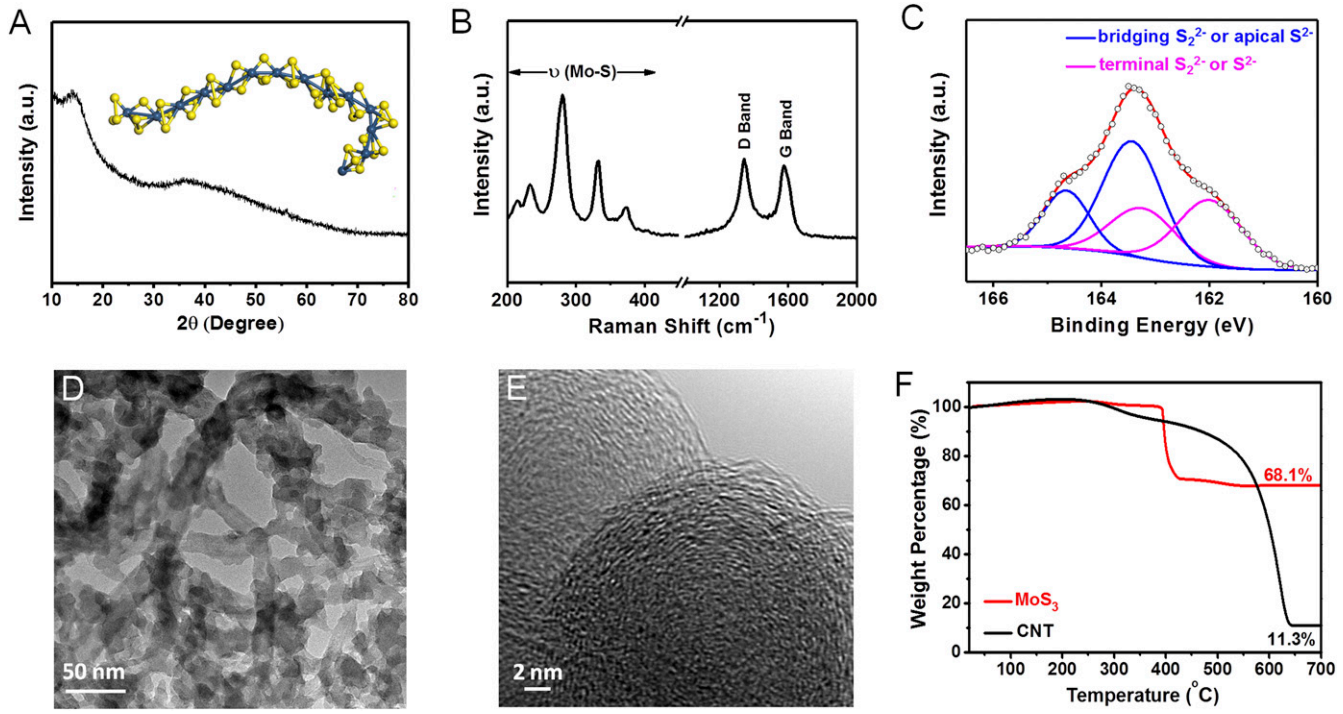

Fig. 2. Structure characterizations of MoS_3. (*A*) XRD pattern. (*Inset*) Schematic structure of 1D chain-like MoS_3. (*B*) Raman spectrum. (*C*) S 2p XPS spectrum. (*D* and *E*) TEM images at different magnifications. (*F*) TGA curve of MoS_3.

capacity of conventional sulfur composites would be lowered to a similar level (400–600 mAh/g) (17–21, 56, 57, 61). Remarkably, our sulfur-equivalent cathode material exhibited an impressive long-term cycling stability. The coin cell after 100 cycles was disassembled, and the used electrolyte was collected and analyzed by UV-visible (UV-vis) spectroscopy. It was free of dissolved polysulfide as commonly observed in cycled Li–S batteries (59, 62–64) (Fig. S2). This result evidenced that the reaction between MoS_3 and Li^+ might not involve the formation of soluble polysulfide intermediates.

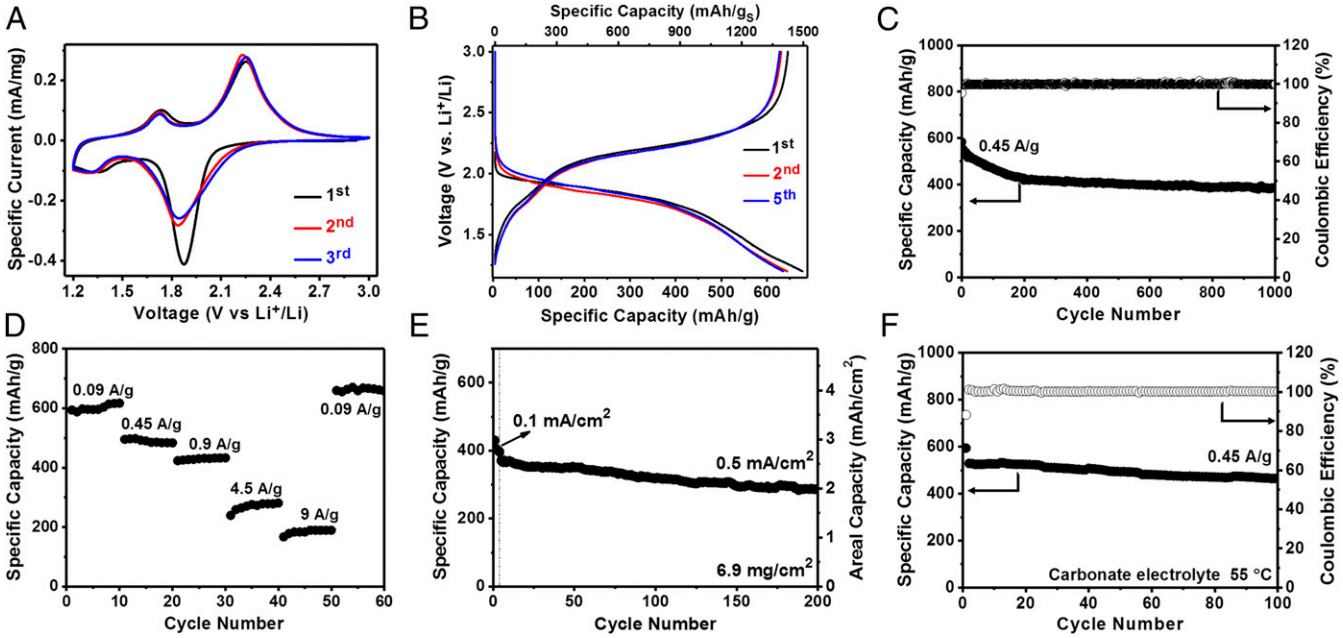

Fig. 3. Electrochemical performances of MoS_3 as the sulfur-equivalent material for Li–S batteries. (*A*) CV curves at the scan rate of 0.1 mV/s. (*B*) Galvanostatic charge and discharge curves at 23 mA/g; specific capacity was normalized to the total mass of MoS_3 (bottom *x* axis) or the mass of S in MoS_3 (top *x* axis). (*C*) Cycling stability and corresponding Coulombic efficiency at 0.45 A/g. (*D*) Rate capability from 0.09 to 9 A/g. (*E*) Cycling stability of a high-loading electrode (6.9 mg/cm^2) at 0.1 mA/cm^2 for the first few cycles and 0.5 mA/cm^2 subsequently. (*F*) Cycling stability and corresponding Coulombic efficiency at 0.45 A/g in the carbonate electrolyte at 55 °C.

Rate capability is the second issue of Li–S batteries due to the insulating nature of elemental sulfur and its full-discharge products (3, 6). Most existing sulfur materials could not achieve appreciable capacities once the current rate went beyond 5 C (18–21, 56, 57, 61). By contrast, our MoS_3 demonstrated decent performance even under very large current rates. When the specific current was ramped from 0.09 A/g to 0.45, 0.9, 4.5, and 9 A/g, its reversible specific capacities gradually lowered from 585 mAh/g to 495, 432, 275, and 189 mAh/g, respectively (Fig. 3*D*). The highest rate of 9 A/g corresponded to a remarkable C rate of ∼12 C, at which charge or discharge was completed within 5 min. Such a high-rate performance was indicative of the rapid reaction kinetics of MoS_3 with Li^+ ions.

Another major concern with Li–S batteries is their deteriorated performance with increasing sulfur loading, and hence very limited areal capacity in general (10, 34). This is because at high sulfur loadings, the dissolution of polysulfide intermediates accelerate. To trap them would require the assistance of more blocking materials, resulting in thick electrode films that are prone to fracture and delaminate from the current collector (5, 6). We demonstrated here that MoS_3 as the sulfur-equivalent cathode material functioned well under high loading. For example, even with 6.9 mg/cm^2 of MoS_3, the electrode delivered high specific capacity of ∼405 mAh/g at 0.1 mA/cm^2 and ∼374 mAh/g at 0.5 mA/cm^2 (Fig. 3*E*). They corresponded to large areal capacities of ∼2.8 and ∼2.6 mAh/cm^2, respectively. In addition, the electrode exhibited great cycling stability at 0.5 mA/cm^2 with ∼78% capacity retention at the end of 200 cycles. The high-loading performance observed here was believed to benefit from the polysulfide-free reaction pathway of MoS_3 and its relatively compact microstructure (low surface area and porosity).

At last, we demonstrated that MoS_3 was cyclable even in carbonate-based electrolyte. Very few sulfur-based materials were able to achieve this because of the rapid reaction between carbonates and polysulfides (9). Here, we switched the electrolyte from 1 M LiTFSI in DOL/DME to 1 M $LiPF_6$ in ethylene carbonate (EC)/dimethyl carbonate (DEC). The CV and galvanostatic charge/discharge curves of MoS_3 in the carbonate electrolyte were very similar to those in the ether electrolyte (Fig. S3 *A* and *B*). At 0.45 A/g, it showed very decent cycling stability with ∼300 mAh/g retained at the end of 1,000 cycles (Fig. S3*C*). Even though such a result was still inferior to the performance in the ether electrolyte, it contrasted conventional Li–S batteries that were completely noncyclable in the carbonate electrolyte, and again evidenced that the reaction between MoS_3 and Li^+ might not involve polysulfide intermediates. The use of carbonate electrolyte was more desirable than ether electrolyte for its lower cost and higher thermal stability (30, 65). For practical applications, it is required that Li–S batteries should be able to work at >55 °C—a temperature that batteries may reach under direct sun exposure in tropical regions (65, 66). Here we showed that MoS_3 in the carbonate electrolyte could cycle well at 55 °C with a measured capacity over 460 mAh/g at the end of 100 cycles (Fig. 3*F*).

From the above assessments, we showed that amorphous MoS_3 as the sulfur-equivalent cathode material provided a possible solution to several long-standing issues of conventional Li–S batteries. It had an electrochemical behavior similar to sulfur but probably did not involve polysulfide intermediates. It was also distinct from transition-metal disulfides (such as those of Mn, Fe, Co, Ni, and many others), which were suggested to lithiate via the conversion reaction mechanism. To gain an insight on the possible lithiation and delithiation mechanism of MoS_3, *operando* X-ray absorption spectroscopy (XAS) was carried out to track the evolution of the oxidation state and coordination environment of Mo and S species during the battery cycling. Fig. 4*A* showed the Mo K-edge X-ray absorption near-edge structure (XANES) spectrum of MoS_3. Its edge position gradually shifted toward lower energy during discharge, suggesting Mo was progressively reduced. The Mo–S bond distance was also monitored via the Fourier transform of the extended X-ray absorption fine-structure (EXAFS) spectrum. It slightly contracted during discharge and then recovered to the original length upon recharge (Fig. 4*B*). S K-edge XANES spectrum of MoS_3 evidenced that sulfur was also reduced during discharge (Fig. 4*C*), but it did not result in the formation of Li_2S or polysulfides (Fig. S4). Based on the above *operando* XAS results, we concluded that the amorphous chain-like structure of MoS_3 was largely preserved during lithiation and delithiation, and that the electrochemical reaction did not involve the formation of any polysulfide. We noted that previously Doan-Nguyen et al. (67) employed *operando* pair-distribution function techniques to track the structural evolution of MoS_3 during lithiation and delithiation, and similarly concluded that the Mo–S bond remained relatively constant upon cycling; Matsuyama et al. (68) also found that both Mo and S in MoS_3 were both redox-active using ex-situ XANES. Our density-functional theory calculations indicated that at discharge the most energetically favorable adsorption site of Li^+ ions was the bridge site between two adjacent sulfur atoms (Fig. 4*D*). With such a configuration, net electron transfer from Li to S and Mo took place.

Encouraged by its outstanding performance for Li–S batteries, we further pursued the possibility of using MoS_3 as the sulfur-equivalent cathode material for room-temperature Na–S batteries. Na–S batteries operate based on the similar electrochemistry as Li–S but are even more challenging. So far, there have been only a handful of reports about room-temperature Na–S batteries, the majority of which have poor cycle life (15, 50, 59, 62, 69). In our experiments, coin-cell-type Na–S batteries were assembled by pairing MoS_3 with a metallic Na disk, filled with 1 M $NaClO_4$ in EC/DEC with 8 vol % fluoroethylene carbonate (FEC) as the electrolyte. Fig. 5*A* shows the galvanostatic charge and discharge curve between 1.0 and 2.8 V. It exhibited a gradual slope between 1.3 and 2.0 V and then a short tail down to 1.0 V. The overall voltage profile resembled those of conventional Na–S batteries (14, 59). Similarly, only subtle modification of the discharge curve before and after the first cycle was noted. The specific capacity of MoS_3 was 460 mAh/g based on the total mass of MoS_3

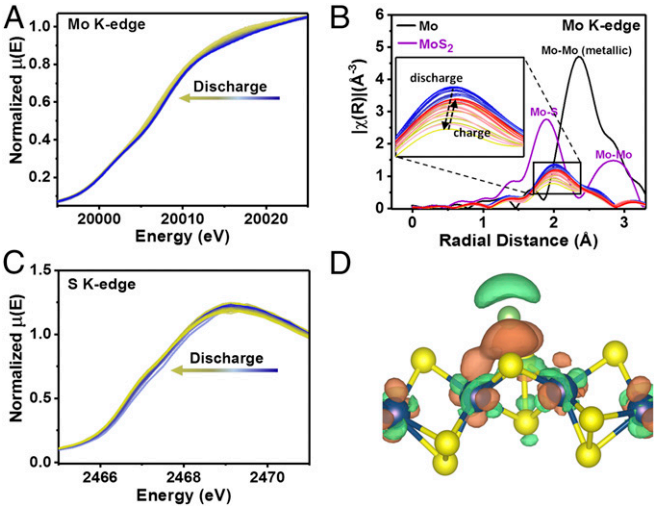

Fig. 4. *Operando* XAS studies of MoS_3 as the sulfur-equivalent cathode material for Li–S batteries. (*A*) Evolution of Mo K-edge XANES spectrum during lithiation. (*B*) Fourier-transformed Mo K-edge EXAFS spectrum of MoS_3 during lithiation and delithiation in comparison with those of MoS_2 and metallic Mo. (*Inset*) Magnified image showing the slight change of Mo–S bond length during the battery cycle. (*C*) Evolution of S K-edge XANES spectrum during lithiation. (*D*) Simulated charge-density distribution in lithiated MoS_3 chains, where cyan, blue, and yellow balls represent Li, Mo, and S atoms, respectively, and green and brick red regions indicate depletion and accumulation of electrons.

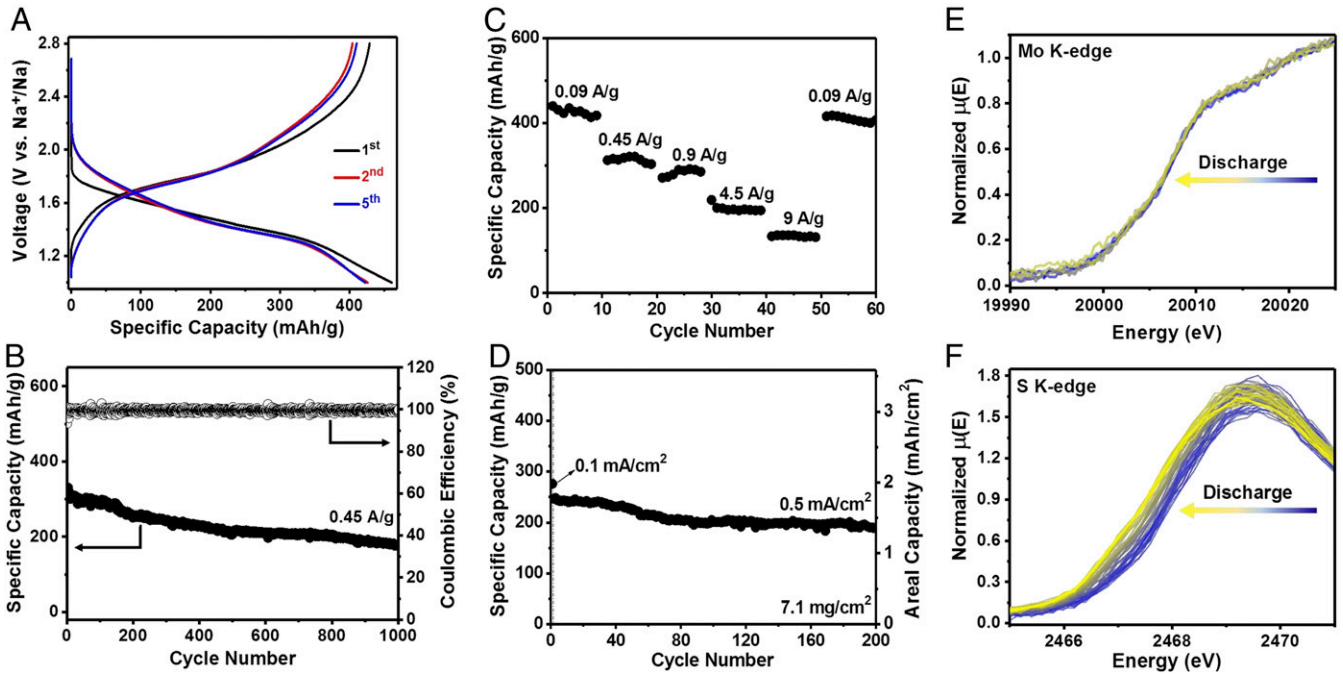

Fig. 5. Electrochemical performances and *operando* XAS studies of MoS_3 as the sulfur-equivalent material for Na–S batteries. (*A*) Galvanostatic charge and discharge curves at 23 mA/g. (*B*) Cycling stability and corresponding Coulombic efficiency at 0.45 A/g. (*C*) Rate capability from 0.09 to 9 A/g. (*D*) Cycling stability of a high-loading electrode (7.1 mg/cm^2) at 0.1 mA/cm^2 for the first few cycles and 0.5 mA/cm^2 subsequently. (*E* and *F*) Evolution of Mo K-edge and S K-edge XANES spectrum during sodiation.

at the first discharge, and 428 mAh/g at subsequent cycles. These values were considerably larger than those of many previous sulfur composite electrodes when their capacities were all normalized to the total composite mass (12–15, 50, 58–60, 69).

MoS_3 demonstrated impressive long-term cycling stability as the sulfur-equivalent cathode material for Na–S batteries. When cycled at 0.45 A/g, its specific capacity slowly decreased but still retained a considerable value of ∼180 mAh/g at the end of 1,000 cycles, and its Coulombic efficiency maintained ∼100% (Fig. 5*B*). By stark contrast, we noted that the reported cycle life of most previous room-temperature Na–S batteries seldom went beyond 200 cycles (12–15, 50, 69). The remarkable long-term cycling stability of our electrode material observed here would be impossible if it was not for the unique structure and electrochemical property of MoS_3. Next, our rate capability assessment evidenced that MoS_3 was also able to uptake Na^+ ions at fast rates. When the specific current was ramped to 4.5 and 9 A/g, the electrode material still sustained significant specific capacities of ∼198 and ∼135 mAh/g, respectively (Fig. 5*C*). Furthermore, we found that increasing the loading of active electrode material did not notably compromise its electrochemical performance. Fig. 5*D* presented the cycling data of MoS_3 with an areal loading of 7.1 mg/cm^2 at 0.5 mA/cm^2. Its specific capacity started at ∼248 mAh/g (corresponding to an areal capacity of 1.76 mAh/cm^2), and had the retention of ∼76% at the end of 200 cycles. This favorable high-loading performance of MoS_3 brought it one step closer to practical applications.

Operando XAS experiments were likewise carried out to study the structural evolution of this sulfur-equivalent cathode material during sodiation and desodiation. Mo K-edge XANES spectrum showed that the shift of its edge position was very slight at discharge (Fig. 5*D*), whereas S K-edge XANES spectrum indicated that the reduction of sulfur was more substantial (Fig. 5*E*), probably due to stronger interaction between Na and S. Fourier-transformed EXAFS of MoS_3 (Fig. 5*F*) revealed that the Mo–S bond was also preserved during repeated sodiation and desodiation without the formation of metallic Mo, Na_2S, or polysulfide (Fig. S5).

Conclusions

In summary, we demonstrated amorphous chain-like MoS_3 as a sulfur-equivalent cathode material for room-temperature sulfur batteries. It was facilely prepared via the acid precipitation method in aqueous solution. In Li–S batteries, MoS_3 exhibited a discharge plateau ∼1.9 V versus Li^+/Li (close to sulfur), large reversible specific capacity, excellent cycle life, and the possibility to achieve high areal capacity. In addition, what clearly distinguished MoS_3 from all previous sulfur-based cathodes was that our material was fully compatible with the carbonate electrolyte with very decent cycling stability, even under a relatively high temperature of 55 °C. *Operando* XAS experiments provided solid evidence that the repetitive lithiation and delithiation of MoS_3 did not cause significant Mo–S bond breaking or Mo–Mo bond formation. There was no Li_2S or polysulfide detected as the reaction intermediate or final product. At last, MoS_3 was also used as the cathode material of Na–S batteries to enable decent capacity and good cycle life. During our investigation, we also explored some other transition-metal polysulfides (such as TiS_3, TiS_4, and NbS_3). They all had much lower working voltage (<1.5 V vs. Li^+/Li) and poorer cycling stability, and therefore were disqualified as the sulfur-equivalent cathode materials. This again highlighted the uniqueness of amorphous MoS_3.

Materials and Methods

Material synthesis, electrode preparation, material characterizations, electrochemical measurements, and *operando* X-ray absorption characterization are detailed in *SI Materials and Methods*.

ACKNOWLEDGMENTS. We acknowledge support from the Ministry of Science and Technology of China (2017YFA0204800), the National Natural Science Foundation of China (51472173 and 51522208), the Natural Science Foundation of Jiangsu Province (BK20140302 and SBK2015010320), the Priority Academic Program Development of Jiangsu Higher Education Institutions, and Collaborative Innovation Center of Suzhou Nano Science and Technology. L.M., T.W., and J.L. acknowledge the financial support from the US Department of Energy under Contract DE-AC02-06CH11357 from the Vehicle Technologies Office, Department of Energy, Office of Energy Efficiency and Renewable Energy.

1. Owens B (2015) Batteries. *Nature* 526:S89–S89.
2. Armand M, Tarascon JM (2008) Building better batteries. *Nature* 451:652–657.
3. Seh ZW, Sun Y, Zhang Q, Cui Y (2016) Designing high-energy lithium-sulfur batteries. *Chem Soc Rev* 45:5605–5634.
4. Evers S, Nazar LF (2013) New approaches for high energy density lithium-sulfur battery cathodes. *Acc Chem Res* 46:1135–1143.
5. Urbonaite S, Poux T, Novák P (2015) Progress towards commercially viable Li-S battery cells. *Adv Energy Mater* 5:1500118.
6. Manthiram A, Fu Y, Chung SH, Zu C, Su YS (2014) Rechargeable lithium-sulfur batteries. *Chem Rev* 114:11751–11787.
7. Yin YX, Xin S, Guo YG, Wan LJ (2013) Lithium-sulfur batteries: Electrochemistry, materials, and prospects. *Angew Chem Int Ed Engl* 52:13186–13200.
8. Yang Y, Zheng G, Cui Y (2013) Nanostructured sulfur cathodes. *Chem Soc Rev* 42: 3018–3032.
9. Zhang S, Ueno K, Dokko K, Watanabe M (2015) Recent advances in electrolytes for lithium-sulfur batteries. *Adv Energy Mater* 5:1500117.
10. Xiao J (2015) Understanding the lithium sulfur battery system at relevant scales. *Adv Energy Mater* 5:1501102.
11. Carbone L, et al. (2015) Comparative study of ether-based electrolytes for application in lithium-sulfur battery. *ACS Appl Mater Interfaces* 7:13859–13865.
12. Manthiram A, Yu X (2015) Ambient temperature sodium-sulfur batteries. *Small* 11: 2108–2114.
13. Wei S, et al. (2016) A stable room-temperature sodium-sulfur battery. *Nat Commun* 7: 11722.
14. Xin S, Yin YX, Guo YG, Wan LJ (2014) A high-energy room-temperature sodium-sulfur battery. *Adv Mater* 26:1261–1265.
15. Wang YX, et al. (2016) Achieving high-performance room-temperature sodium-sulfur batteries with S@interconnected mesoporous carbon hollow nanospheres. *J Am Chem Soc* 138:16576–16579.
16. Ji X, Lee KT, Nazar LF (2009) A highly ordered nanostructured carbon-sulphur cathode for lithium-sulphur batteries. *Nat Mater* 8:500–506.
17. Liu W, et al. (2017) Ultrathin dendrimer-graphene oxide composite film for stable cycling lithium-sulfur batteries. *Proc Natl Acad Sci USA* 114:3578–3583.
18. Ji L, et al. (2011) Graphene oxide as a sulfur immobilizer in high performance lithium/sulfur cells. *J Am Chem Soc* 133:18522–18525.
19. Zhou G, et al. (2012) A flexible nanostructured sulphur–carbon nanotube cathode with high rate performance for Li-S batteries. *Energy Environ Sci* 5:8901.
20. Li Z, Zhang J, Lou XW (2015) Hollow carbon nanofibers filled with MnO_2 nanosheets as efficient sulfur hosts for lithium-sulfur batteries. *Angew Chem Int Ed Engl* 54: 12886–12890.
21. Wei Seh Z, et al. (2013) Sulphur-TiO_2 yolk-shell nanoarchitecture with internal void space for long-cycle lithium-sulphur batteries. *Nat Commun* 4:1331.
22. Han X, et al. (2013) Reactivation of dissolved polysulfides in Li–S batteries based on atomic layer deposition of Al_2O_3 in nanoporous carbon cloth. *Nano Energy* 2: 1197–1206.
23. Zhang Q, et al. (2015) Understanding the anchoring effect of two-dimensional layered materials for lithium-sulfur batteries. *Nano Lett* 15:3780–3786.
24. Zhong Y, et al. (2017) Mechanistic insights into surface chemical interactions between lithium polysulfides and transition metal oxides. *J Phys Chem C* 121:14222–14227.
25. Fang X, Peng H (2015) A revolution in electrodes: Recent progress in rechargeable lithium-sulfur batteries. *Small* 11:1488–1511.
26. Seh ZW, et al. (2014) Two-dimensional layered transition metal disulphides for effective encapsulation of high-capacity lithium sulphide cathodes. *Nat Commun* 5: 5017.
27. Jiang J, et al. (2015) Encapsulation of sulfur with thin-layered nickel-based hydroxides for long-cyclic lithium-sulfur cells. *Nat Commun* 6:8622.
28. Niu XQ, et al. (2015) Metal hydroxide–a new stabilizer for the construction of sulfur/carbon composites as high-performance cathode materials for lithium–sulfur batteries. *J Mater Chem A* 3:17106–17112.
29. Li W, et al. (2013) High-performance hollow sulfur nanostructured battery cathode through a scalable, room temperature, one-step, bottom-up approach. *Proc Natl Acad Sci USA* 110:7148–7153.
30. Li W, et al. (2013) Understanding the role of different conductive polymers in improving the nanostructured sulfur cathode performance. *Nano Lett* 13:5534–5540.
31. Chung S-H, Manthiram A (2014) Bifunctional separator with a light-weight carbon-coating for dynamically and statically stable lithium-sulfur batteries. *Adv Funct Mater* 24:5299–5306.
32. Su YS, Manthiram A (2012) A new approach to improve cycle performance of rechargeable lithium-sulfur batteries by inserting a free-standing MWCNT interlayer. *Chem Commun* 48:8817–8819.
33. Jin Z, Xie K, Hong X, Hu Z, Liu X (2012) Application of lithiated Nafion ionomer film as functional separator for lithium sulfur cells. *J Power Sources* 218:163–167.
34. Hagen M, et al. (2015) Lithium-sulfur cells: The gap between the state-of-the-art and the requirements for high energy battery cells. *Adv Energy Mater* 5:1401986.
35. Wu M, et al. (2016) Organotrisulfide: A high capacity cathode material for rechargeable lithium batteries. *Angew Chem Int Ed Engl* 55:10027–10031.
36. Liu M, Visco SJ, De Jonghe LC (1989) Electrochemical properties of organic disulfide thiolate redox. *J Electrochem Soc* 136:2570–2575.
37. Oyama N, Tatsuma T, Sato T, Sotomura T (1995) Dimercaptan-polyaniline composite electrodes for lithium batteries with high energy density. *Nature* 373:598–600.
38. Wang J, Yang J, Xie J, Xu N (2002) A novel conductive polymer-sulfur composite for rechargeable lithium batteries. *Adv Mater* 14:963–965.
39. Cao X, Tan C, Zhang X, Zhao W, Zhang H (2016) Solution-processed two-dimensional metal dichalcogenide-based nanomaterials for energy storage and conversion. *Adv Mater* 28:6167–6196.
40. Stephenson T, Li Z, Olsen B, Mitlin D (2014) Lithium ion battery applications of molybdenum disulfide (MoS_2) nanocomposites. *Energy Environ Sci* 7:209–231.
41. Liu Y, et al. (2016) Electrical, mechanical, and capacity percolation leads to high-performance MoS_2/nanotube composite lithium ion battery electrodes. *ACS Nano* 10: 5980–5990.
42. Liu Y, et al. (2016) Liquid phase exfoliated MoS_2 nanosheets percolated with carbon nanotubes for high volumetric/areal capacity sodium-ion batteries. *ACS Nano* 10: 8821–8828.
43. Xiao J, et al. (2011) Electrochemically induced high capacity displacement reaction of PEO/MoS_2/graphene nanocomposites with lithium. *Adv Funct Mater* 21:2840–2846.
44. Xu X, Liu W, Kim Y, Cho J (2014) Nanostructured transition metal sulfides for lithium ion batteries: Progress and challenges. *Nano Today* 9:604–630.
45. Li X, et al. (2016) Regeneration of metal sulfides in the delithiation process: The key to cyclic stability. *Adv Energy Mater* 6:1601056.
46. Fang X, et al. (2012) Mechanism of lithium storage in MoS_2 and the feasibility of using Li_2S/Mo nanocomposites as cathode materials for lithium-sulfur batteries. *Chem Asian J* 7:1013–1017.
47. Hibble SJ, Wood GB (2004) Modeling the structure of amorphous MoS_3: A neutron diffraction and reverse Monte Carlo study. *J Am Chem Soc* 126:959–965.
48. Weber T, Muijsers JC, Niemantsverdriet JW (1995) Structure of amorphous MoS_3. *J Phys Chem* 99:9194–9200.
49. Jacobson AJ, Chianelli RR, Rich SM, Whittingham MS (1979) Amorphous molybdenum trisulfide: A new lithium battery cathode. *Mater Res Bull* 14:1437–1448.
50. Zheng S, et al. (2014) Nano-copper-assisted immobilization of sulfur in high-surface-area mesoporous carbon cathodes for room temperature Na-S batteries. *Adv Energy Mater* 4:1400226.
51. Schleich DM, Chang HS (1989) MoS_3 thin film cathodes prepared by chemical vapor deposition. *J Electrochem Soc* 136:3274–3278.
52. Ye H, et al. (2017) Amorphous MoS_3 infiltrated with carbon nanotubes as an advanced anode material of sodium-ion batteries with large gravimetric, areal, and volumetric capacities. *Adv Energy Mater* 7:1601602.
53. Zhang W, et al. (2015) Water-soluble MoS_3 nanoparticles for photocatalytic H_2 evolution. *ChemSusChem* 8:1464–1471.
54. Sourisseau C, Gorochov O, Schleich DM (1989) Comparative IR and Raman studies of various amorphous MoS_3 and Li_xMoS_3 phases. *Mater Sci Eng B* 3:113–117.
55. Merki D, Fierro S, Vrubel H, Hu X (2011) Amorphous molybdenum sulfide films as catalysts for electrochemical hydrogen production in water. *Chem Sci* 2:1262–1267.
56. Xin S, et al. (2012) Smaller sulfur molecules promise better lithium-sulfur batteries. *J Am Chem Soc* 134:18510–18513.
57. Lei T, et al. (2016) Multi-functional layered WS_2 nanosheets for enhancing the performance of lithium-sulfur batteries. *Adv Energy Mater* 7:1601843.
58. Hwang TH, Jung DS, Kim JS, Kim BG, Choi JW (2013) One-dimensional carbon-sulfur composite fibers for Na-S rechargeable batteries operating at room temperature. *Nano Lett* 13:4532–4538.
59. Fan L, Ma R, Yang Y, Chen S, Lu B (2016) Covalent sulfur for advanced room temperature sodium-sulfur batteries. *Nano Energy* 28:304–310.
60. Qiang Z, et al. (2017) Ultra-long cycle life, low-cost room temperature sodium-sulfur batteries enabled by highly doped (N,S) nanoporous carbons. *Nano Energy* 32:59–66.
61. Demir-Cakan R, et al. (2011) Cathode composites for Li-S batteries via the use of oxygenated porous architectures. *J Am Chem Soc* 133:16154–16160.
62. Peng HJ, et al. (2016) Janus separator of polypropylene-supported cellular graphene framework for sulfur cathodes with high utilization in lithium-sulfur batteries. *Adv Sci* 3:1500268.
63. Yao H, et al. (2014) Improved lithium–sulfur batteries with a conductive coating on the separator to prevent the accumulation of inactive s-related species at the cathode–separator interface. *Energy Environ Sci* 7:3381–3390.
64. Li Z, et al. (2016) A sulfur host based on titanium monoxide@carbon hollow spheres for advanced lithium-sulfur batteries. *Nat Commun* 7:13065.
65. Li X, et al. (2016) Safe and durable high-temperature lithium-sulfur batteries via molecular layer deposited coating. *Nano Lett* 16:3545–3549.
66. Tarascon JM, Armand M (2001) Issues and challenges facing rechargeable lithium batteries. *Nature* 414:359–367.
67. Doan-Nguyen VVT, et al. (2016) Molybdenum polysulfide chalcogels as high-capacity, anion-redox-driven electrode materials for Li-ion batteries. *Chem Mater* 28: 8357–8365.
68. Matsuyama T, et al. (2016) Structure analyses using X-ray photoelectron spectroscopy and X-ray absorption near edge structure for amorphous MS_3 (M: Ti, Mo) electrodes in all-solid-state lithium batteries. *J Power Sources* 313:104–111.
69. Yu X, Manthiram A (2015) Ambient-temperature sodium-sulfur batteries with a sodiated Nafion membrane and a carbon nanofiber-activated carbon composite electrode. *Adv Energy Mater* 5:1500350.
70. Ye H, et al. (2016) Iron-based sodium-ion full batteries. *J Mater Chem A* 4:1754–1761.